Synthesis and characterization of ZnO nanoparticle synthesized by a microwave-assisted combustion method and catalytic activity for the removal of ortho-nitrophenol

Navid Assi[a], Ali Mohammadi[a,b,*], Qazale Sadr Manuchehri[a], Roderick B. Walker[c]

[a]Faculty of Pharmacy, Department of Drug & Food Control, Tehran University of Medical Sciences, P.O.Box:14155-6451, Tehran, Iran. Tel. +98 2164122163; Fax: +98 2166461178; email: alimohammadi@tums.ac.ir
[b]Faculty of Pharmacy, Nanotechnology Research Centre, Tehran University of Medical Sciences, Tehran, Iran
[c]Faculty of Pharmacy, Rhodes University, Grahamstown 6140, South Africa

ABSTRACT

ZnO nanoparticles were manufactured using microwave-assisted combustion. The structural and morphological properties of the nanoparticles were characterized by X-ray diffraction (XRD), field emission scanning electron microscopy, and Fourier transform infrared spectroscopy. Photocatalytic degradation of ortho-nitrophenol (O-NP) in aqueous solution using the synthesized nanoparticles was performed under UV–C irradiation and is reported for the first time. The effect of the initial O-NP concentration, amount of photocatalyst, pH, and salt was investigated during photodegradation. Analysis of the degraded samples using HPLC with UV detection revealed that photocatalysis in the presence of ZnO nanoparticles removed 98% of the O-NP in 5 h. In addition, the photocatalytic degradation kinetics of O-NP were studied, and the results suggest that the data are best fitted to pseudo-first-order kinetic and Langmuir–Hinshelwood models.

Keywords: Microwave-assisted combustion; ZnO nanoparticles; Ortho-nitrophenol; Photocatalytic degradation

1. Introduction

Nitrophenol and derivatives thereof are used in the manufacture of biorefractory organic compounds, synthetic dyes, petrochemicals, pharmaceuticals (e.g. acetaminophen), pesticides (e.g. methyl and ethyl parathion), leather treatment and for military purposes [1–3]. These compounds are highly toxic, carcinogenic and exhibit mutagenic effects [4] and are considered priority pollutants by the United States Environmental Protection Agency [5–8]. Many processes have been developed for the removal of these compounds from the environment and include adsorption [9], microbial [10] or photocatalytic degradation [11], microwave-assisted catalytic oxidation [12], electro-Fenton methods [13], electrocoagulation [14], electrochemical treatment [15], and advanced oxidation using UV/H_2O_2 [16,17]. Heterogeneous photocatalysis is an important destructive technology leading to the total mineralization of most organic pollutants [18]. Some metal oxide semiconductors such as titanium dioxide (TiO_2), zinc oxide (ZnO), tungsten oxide (WO_3), strontium titanate ($SrTiO_3$), and hematite (α-Fe_2O_3) are

*Corresponding author.

purported to be dynamic photocatalysis [19] Due to their high photosensitivity, chemical stability, and low toxicity, TiO_2 and ZnO have been especially investigated for the sequestration and/or degradation of a number of environmental pollutants [20,21]. ZnO has been reported to be more efficient than TiO_2 under certain conditions when used for photocatalytic oxidation of pulp mill bleach wastewater to remove 2-phenylphenol and phenol [22]. The use of ZnO covers a wide range of applications due to its ability to absorb ultra-violet radiation, act as a photocatalyst or photo-detectors as a result of it is a wide band gap (3.37ev) and high excitation binding energy (60 mV) [23,24]. ZnO nanoparticles can be synthesized by a number of techniques including sol–gel processing [25,26], homogeneous precipitation [27], mechanical milling [28], organometallic synthesis [29], microwave [30], spray pyrolysis [31,32], thermal evaporation [33], or mechanochemical synthesis [34].

Microwave-assisted synthesis has attracted much attention since it is a rapid, simple and highly energy efficient approach. In this process, a precursor solution is irradiated by a microwave source and efficient energy transfers through either resonance or relaxation which can result in rapid and homogenous heating of the precursor solution in a short time resulting in uniform particle size distribution [35].

In this study, we report the manufacture of ZnO nanoparticles using a microwave-assisted combustion method, the optimization of synthetic parameters and the morphological characterization of the particles. In addition, we report the use of ZnO nanoparticles under optimized photodegradation conditions for the photocatalysis of O-NP is reported, for the first time.

2. Experimental

2.1. Materials and reagents

O-NP($C_6H_5NO_3$), zinc nitrate hexahydrate (Zn$(NO_3)_2 \cdot 6H_2O$), citric acid ($C_6H_8O_7$), hydrochloric acid (HCl), and ammonia solution (25% v/v) were obtained from Merck (Germany). All materials were of analytical grade and were used without any further purification. Deionized water was used for the preparation of all the samples.

2.2. Preparation of ZnO nanoparticles

The ratio of Zn$(NO_3)_2 \cdot 6H_2O$ to citric acid was fixed in a 1:3 mol ratio, and the compounds were dissolved in a minimum volume of deionized water to produce an clear solution. The ammonia solution (25% v/v) was added dropwise to adjust the pH of the solution to 4. The solution was then allowed to evaporate with continuous stirring for 6 h on a water bath maintained at 60°C. After the water had evaporated, the resultant gel was exposed to microwave irradiation at a power of 900 W for 10 min (Fig. 1). The resultant powder was collected and cleaned by washing with deionized water on two occasions. The precursor powder was then calcined at 800°C for 2 h to produce the ZnO nanoparticles.

2.3. Assessment of photocatalytic activity of ZnO

In order to assess the photocatalytic activity of ZnO nanoparticles, a O-NP solution was prepared by dissolving 0.002 g O-NP in 200 mL deionized water and transferred to clean containers. This solution was used as a test contaminant for determining the photocatalytic activity of the ZnO nanoparticles.

About 0.05 g quantity of the nanophotocatalyst was added to each of the containers containing the O-NP solution. The solutions were placed at a distance of 10 cm from the UV–C lamp and irradiated at a power of 30 W for 300 min with continuous agitation. Aliquots of each sample were removed from the test solutions and centrifugation at 2,200 rpm for 20 min in order to completely remove all nanoparticles. The resultant clear, transparent supernatant solutions were analyzed to determine the amount of O-NP that remained in solution.

Fig. 1. Microwave product produced at a power of 900 W for 10 min.

2.4. Analytical methods

The extent of the degradation of O-NP was established using UV–vis spectrophotometer (PER-KIN-ELMER, Lambda15) and HPLC (Knauer, Pump K-1,001, a UV Detector K-2600) at a λ_{max} of 279 nm.

3. Results and discussion

3.1. Characterization of synthesized photocatalyst

X-ray diffraction (XRD) patterns were captured using a D8-Advance (Product Cooperation Bruker AXS and Siemens) fitted with a Cu (Kα) radiation tube. The phase and purity of the nanoparticles were established by interpretation of the XRD patterns (Fig. 2). The presence of well-defined sharp peaks indicates the degree of crystalline quality and confirms the formation and the presence of a single phase of the zinc oxide nanoparticles. The diffraction peaks can be indexed by comparison to a the pattern observed for the ZnO standard viz. zinc white, 00–005-0,664. The average crystalline size calculated using the

Debeye–Scherrer equation Eq. 1 was established to be 38 nm with a degree of crystallinity of 93%.

$$D = \frac{0.89.\lambda}{\beta \cdot cos\theta} \tag{1}$$

where D = average size of the crystal in nm; λ = wavelength of the X-rays; β = the full width of the peak at half maximum; θ = half diffraction angle.

FE-SEM images of the zinc oxide nanoparticles were generated using a Hitachi S4160 microscope with a resolution of 300,000 in the cold field emission mode and are shown in Figs. 3(a) and (b). In comparison with the standard patterns observed, the morphology of the ZnO nanoparticles produced by microwave-assisted combustion reveals the presence of nanorods Fig. 3(a) and hexagonal cross sections Fig. 3(b).

FT-IR spectroscopy is a powerful and useful technique that has been used to analyze, confirm, and elucidate the chemical structure of compounds and to identify functional groups that are present in the
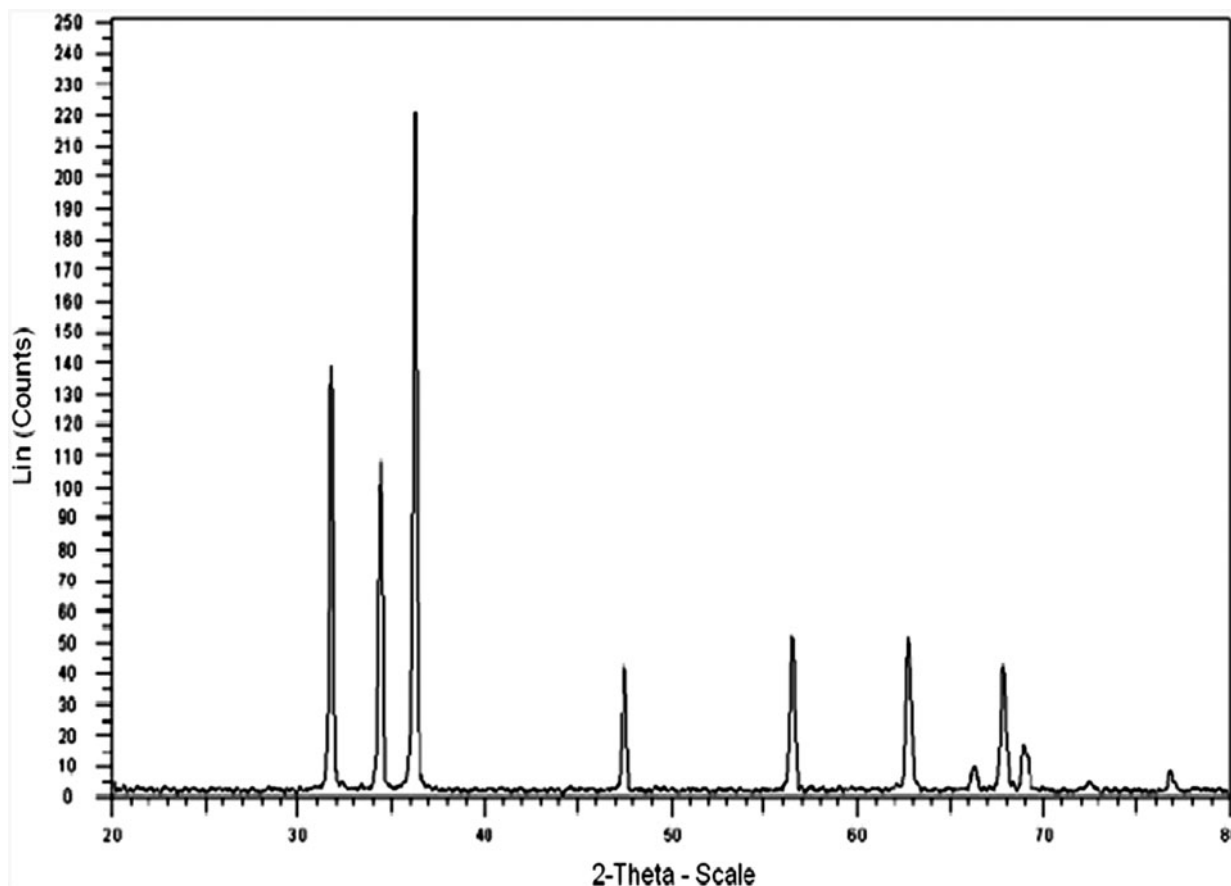
Fig. 2. XRD spectrum of ZnO following synthesis with microwave-assisted combustion.
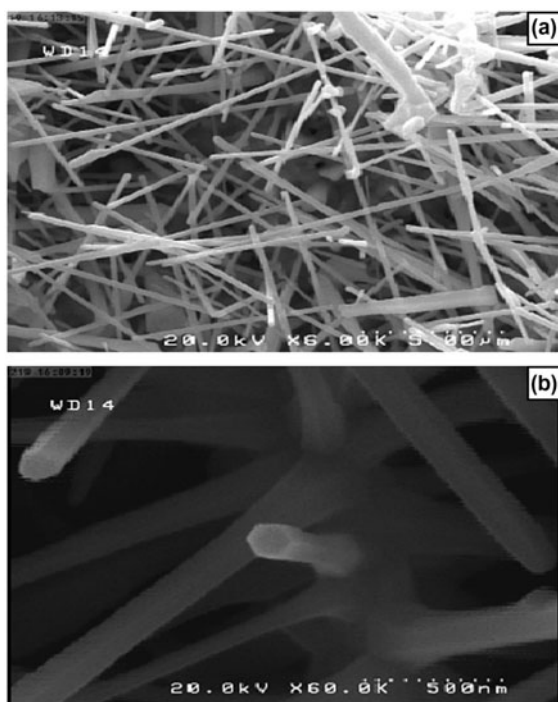
Fig. 3. (a) FE-SEM micrograph of ZnO synthesized using microwave-assisted combustion, (b) hexagonal cross section area.

molecule. The FT-IR spectra of the ZnO nanoparticles were influenced by the particle size and morphology of the materials. The FT-IR spectra of the ZnO nanoparticles synthesized in this study are depicted in Fig. 4. The peak observed at 425–520 cm^{-1} corresponds to the Zn–O stretching mode [36].

3.2. Photocatalytic efficiency of synthesized ZnO nanoparticles

Photocatalytic degradation of ZnO was performed with UV–C irradiation and monitored by the use of an optical absorption spectrophotometer. The photodegradation studies using O-NP in a solution of pH of 7 at a concentration of 10 mg L^{-1} was undertaken using 0.05 g of the ZnO nanoparticles, and the resultant absorption spectrum was depicted in Fig. 5 that shows the reduction in the intensity of the peaks over 300 min.

The removal of O-NP was < 7% in the presence ZnO nanoparticles stored in a dark place and was 20% when exposed to UV–C irradiation only. As depicted in Fig. 6, it is clearly evident that exposure of O-NP in the presence of the ZnO nanoparticles to UV–C irradiation resulted in almost complete degradation (98%) of the O-NP in 300 min. These observations reveal that there is synergistic activity when UV light and ZnO nanoparticles are used to degrade O-NP and the extent of degradation of O-NP can calculated using Eq. (2):

$$X = \frac{A^0 - A}{A^0} \times 100 \qquad (2)$$

where X = percent degradation, A^0 = initial value for absorption, and A = absorption at any time after exposure peaks over.

When a photocatalyst is irradiated by a light source that stronger than the band gap energy for that compound, electron hole pairs diffuse from the surface of the photocatalyst and are able to participate in

Fig. 4. FT-IR spectrum of ZnO nanoparticles prepared using microwave assisted combustion.
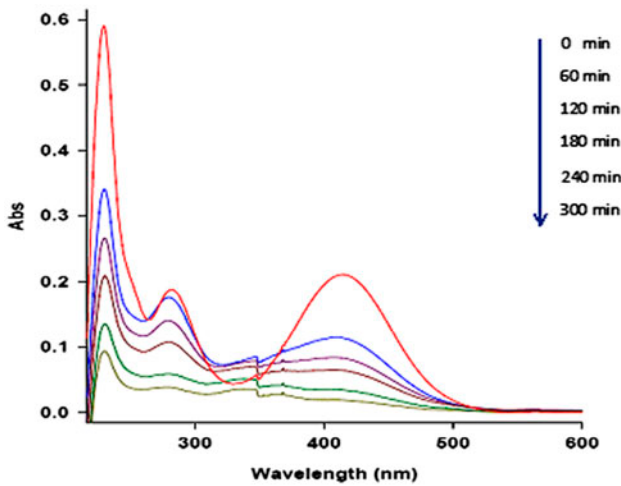
Fig. 5. Absorption spectrum following photodegradation of O-NP = 10 mg L^{-1}, pH = 7, in the presence of 0.05 g ZnO nanoparticles using UV–C irradiation.

chemical reactions with an electron donor and acceptor. The free electrons and holes transform surrounding oxygen or water molecules into hydroxyl free radicals (OH$^{\bullet}$) with super strong oxidizing capability that oxygenolyse different organic compounds and in some cases, minerals. Examples of the reactions are depicted in Eqs. (3)–(5) [22,37].

$$ZnO + hv \rightarrow ZnO \; (eCB^{-} + hVB^{+}) \tag{3}$$

$$eCB^{-} + O_2 \rightarrow O_2^{-\bullet} \tag{4}$$

$$hVB^{+} + H_2O \rightarrow H^{+} + OH^{\bullet} \tag{5}$$
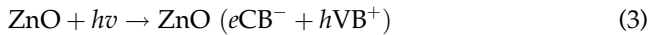
3.2.1. Effect of ZnO loading

The amount of photocatalyst required is an important parameter that affects the rate of degradation of pollutant. Therefore, O-NP degradation was investigated at four levels of amount of ZnO nanoparticles, and the results of these studies are depicted in Fig. 7. It is evident that the photocatalytic degradation of O-NP increases with an increase in the amount of ZnO nanoparticles added up to a limit of 0.05 g after which there is no additional or significant degradation. This observation can, in part, be explained in respect of the availability of active sites on the surface of the catalyst and the limited penetration of UV radiation into the suspension. The total number of active sites and surface area increases as the amount of catalyst used increases; however, there is a corresponding increase in the turbidity of the suspension with an associated decrease in extent to which UV light can penetrate the suspension, and with an increased scattering effect, there is a decrease in the photo-activated volume of the suspension. Furthermore, at high levels of catalyst loading, it is difficult to maintain an homogenous suspension due to particle agglomeration which further decreases the number of active sites available in the system [37–40]. Consequently, 0.05 g of ZnO particles was used for all additional studies.
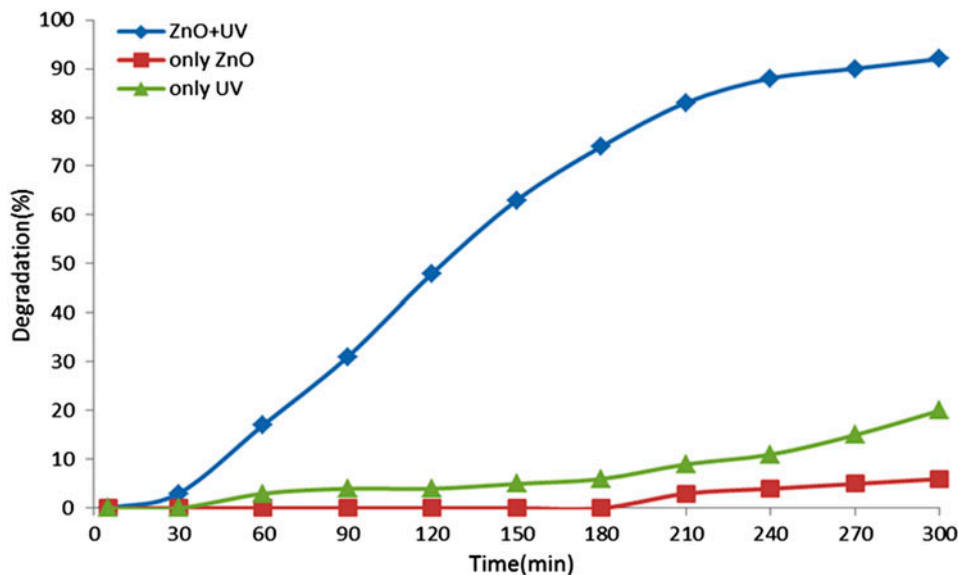
Fig. 6. Effect of UV light and ZnO nanoparticles (0.05 g) on the photocatalytic degradation of O-NP = 10 mg L^{-1}.
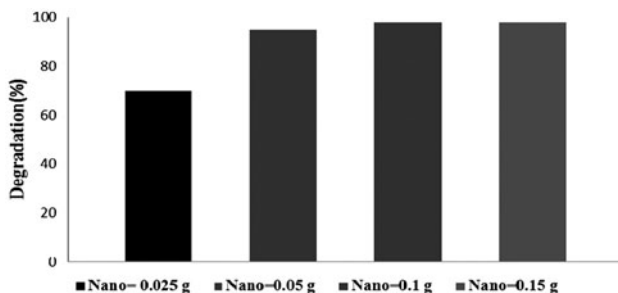
Fig. 7. Effect of amount of ZnO nanoparticles on photocatalytic degradation efficiency of O-NP = 10 mg L^{-1} at pH = 7 after 300 min exposure.

3.2.2. Effect of initial O-NP concentration

The initial concentration of O-NP has an impact on the extent of photocatalytic degradation, and therefore, initial loading was investigated at four concentrations between 5 and 20 mg L^{-1}, and the results of these studies are depicted in Fig. 8. It is evident that as the initial concentration of O-NP increase so the extent of photocatalytic degradation decreases as more O-NP is adsorbed onto the surface of photocatalyst resulting in low availability of active sites for the adsorption of hydroxyl ions, thereby limiting the generation of hydroxyl radicals. Furthermore, as the initial concentration of O-NP in solution increases, photons are adsorbed by the O-NP prior to reaching the surface of the catalyst reducing the uptake of photons by the nanocatalyst resulting in a reduction in the extent of degradation observed [37–41].

3.2.3. Effect of pH

The pH of solutions can have a significant impact on photocatalytic processes [42,43]. Therefore, the effect of pH of solution on the degradation of O-NP was studied over the range of 3–11. The effect of pH on the degradation of O-NP at a fixed reaction time of 300 min is depicted in Fig. 9. The results indicate that the degradation of O-NP was best achieved in a solution of pH = 7. The zero-point charge for ZnO is 9, and ZnO has a positive charge [22]. The pKa of O-NP is 7.16, and in a solution of pH = 7, the compound is negatively charged resulting in a high degree of adsorption due to electrostatic forces, at this pH.

3.2.4. Effect of salt

The effect of ionic strength by inclusion of sodium chloride (NaCl) on the rate and extent of photocatalytic degradation of O-NP in the presence of ZnO nanoparticles was studied, and the results are
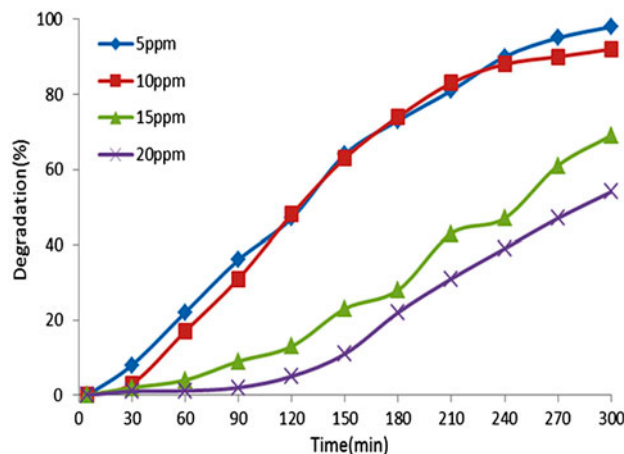
Fig. 8. Effect of initial concentration of O-NP on the extent of photocatalytic degradation of O-NP in the presence of ZnO = 0. 05 g at pH = 7 after 300 min exposure.

depicted in Fig. 10. The inclusion of NaCl did not enhance the degradation of O-NP possibly due to the hydroxyl radical inhibition effect of the chloride ion as depicted in the reactions described by Eqs. (6) and (7) [44].

$$Cl^- + OH^\bullet \rightarrow HOCl^{\bullet-} \tag{6}$$

$$HOCl^{\bullet-} + H^+ \rightarrow Cl^\bullet + H_2O \tag{7}$$
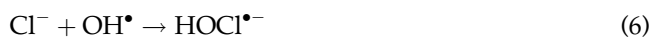
The presence of NaCl can decrease the extent of photocatalytic degradation of O-NP.

3.3. HPLC monitoring of O-NP degradation

HPLC with UV detection was used to determine the amount of O-NP that degraded and to establish
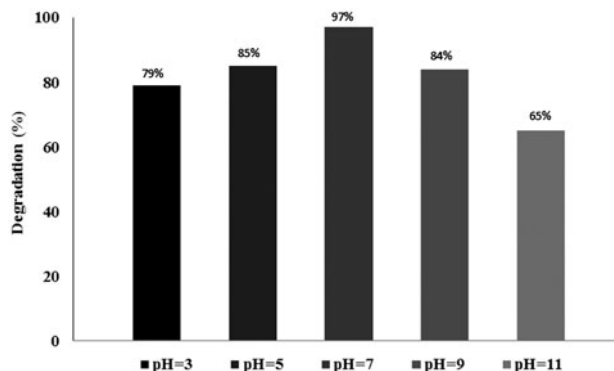
Fig. 9. The effect of pH on the photocatalytic degradation of O-NP = 10 mg L^{-1} in the presence of ZnO (0.05 g) after 300 min exposure.
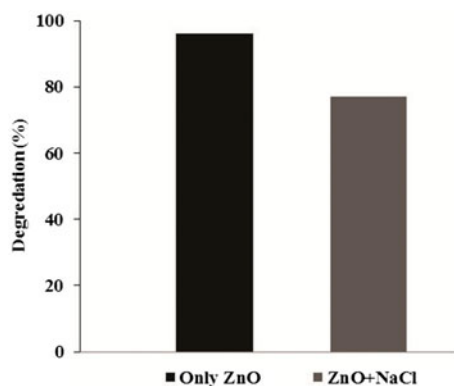
Fig. 10. The Effect of sodium chloride on the degradation of O-NP = 10 mg L^{-1}, ZnO = 0. 05 g, pH = 7, NaCl = 5 g.

that no degradation by products were present. The modular HPLC system consisted of a Knauer HPLC Pump K-1,001, a UV Detector K-2,600, a Knauer injection system and a Knauer solvent degasser (Berlin, Germany). ChromGate® Chromatography Data System Version 3.1.7 (Berlin, Germany) was used to capture and evaluate the data following chromatographic analysis. The chromatographic separation was optimized on a Perfectsil® Target ODS, 3–5 μm, 125 × 4 mm i.d. column using a mobile phase consisting of ethanol–50 mM ammonium acetate buffer (pH = 3.7) in a ratio of

40:60, v/v at a flow rate of 0.7 ml/min with UV detection at 290 nm. As depicted in Fig. 11, the retention time of O-NP and its primary degradation products were 12 and 7 min, respectively. In excess of 98% degradation was observed after 300 min exposure, and neither O-NP nor degradation by-products was detectable following photodegradation under these conditions for 300 min.

3.4. Kinetics of photocatalytic degradation of O-NP

The effect of initial concentration of O-NP on the degradation rate of the compound was studied in the concentration range 5–20 mg L^{-1}. A plot of a the negative log of the ratio of concentration to the original concentration as described by Eq. (8) will produce a straight line for $-\ln(C/C_0)$ vs. time (t) and describes a pseudo-first-order kinetic relationship [45].

$$-\ln \frac{C}{C_0} = kt \tag{8}$$

Pseudo-first-order degradation curves are depicted in Fig. 12, and the resultant correlation coefficients (R^2) for these studies ranged between 0.9661 and 0.9893 for all concentrations investigated, indicating that the degradation of O-NP followed a pseudo-first-order kinetic model.
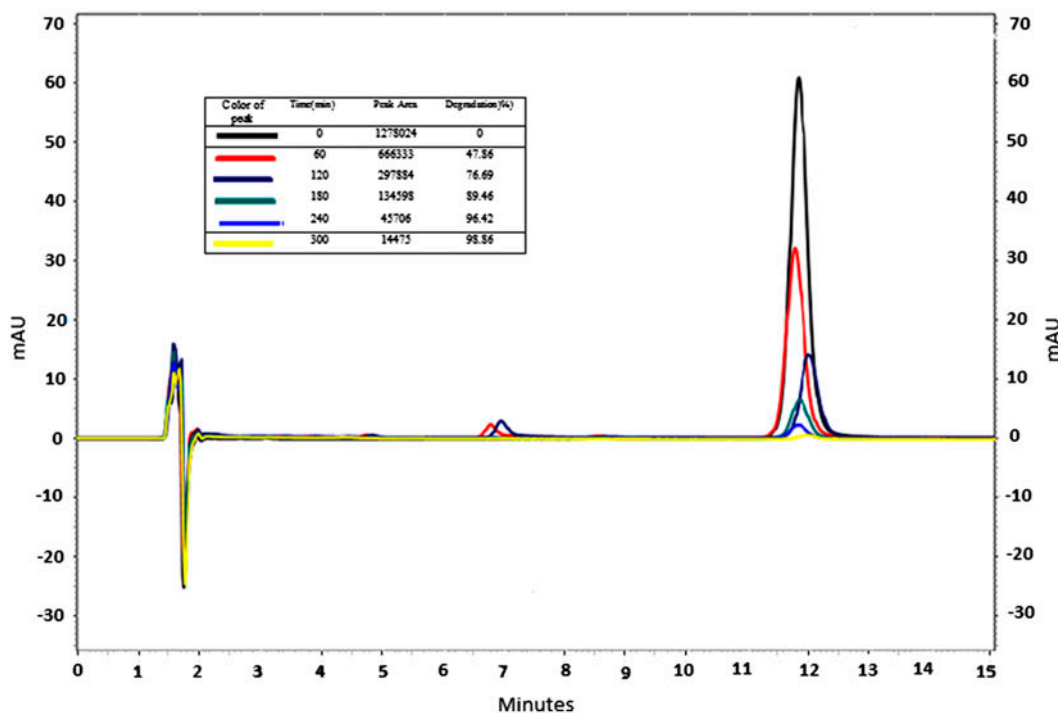
Fig. 11. HPLC chromatograms for samples following photocatalytic degradation of O-NP.
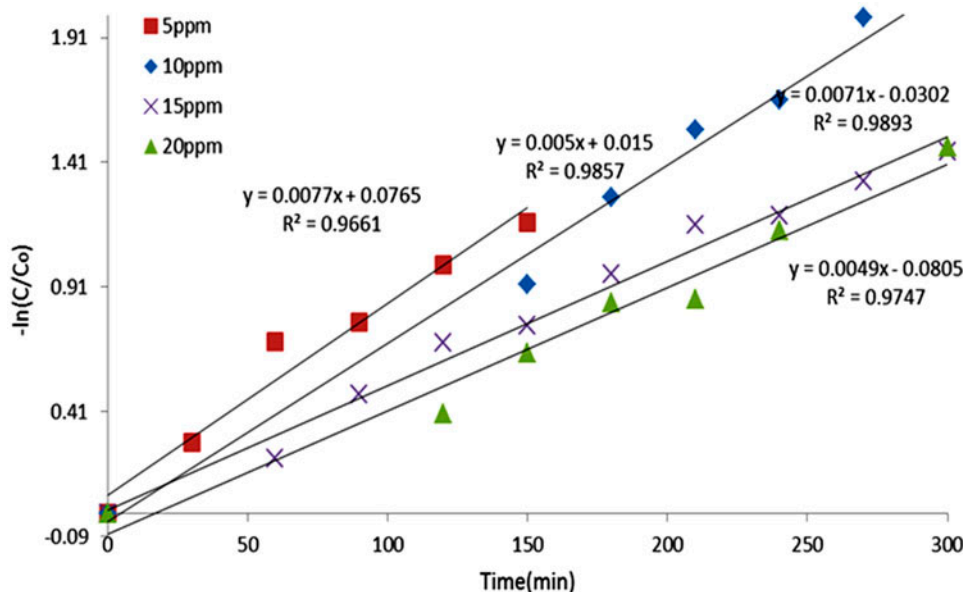
Fig. 12. First-order plots for photocatalytic degradation of O-NP using different initial concentrations of the compound.

Using methodology proposed by different authors [21], the results permit a semi-quantitative analysis of these data by comparison of the apparent rate constants determined from photodegradation reactions. In general, pseudo-first-order kinetic process and in this case photocatalytic degradation follow the Langmuir–Hinshelwood mechanism with the result that the reaction rate is proportional to amount of photocatalytic material covered (θ) with the pollutant viz. O-NP:

$$r_0 = k_r\theta = -\frac{dC}{dt} = \frac{k_rK_aC_0}{1 + K_aC_0} \tag{9}$$
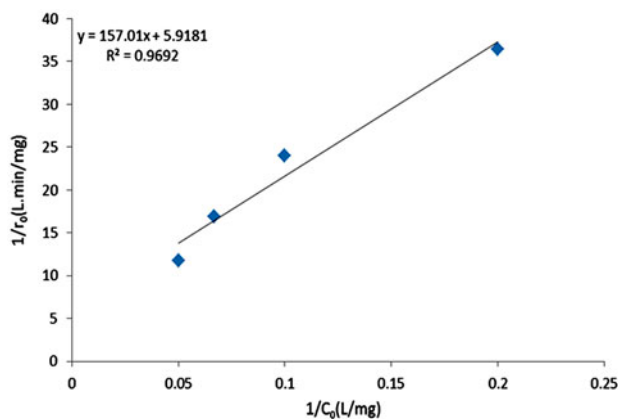
Fig. 13. A plot of $1/r_0$ against $1/C_0$ for the catalysis of O-NP.

where k_r = the true rate constant including parameters such as catalyst loading, photonflux, and oxygen coverage, K_a = the adsorption constant, θ = amount of photcatalytic material covered, C_0 = initial concentration.

Since photocatalytic reactions can occur only when organic pollutant molecules are adsorbed onto the surface of a catalyst and evaluation of the values of K_r and K_a are important. Modification of Eq. 9 by use of reciprocal numbers on both sides of the equation yields Eq. (10) [46].

$$\frac{1}{r_0} = \frac{1 + k_aC_0}{k_rK_aC_0} = \frac{1}{k_rK_aC_0} + \frac{1}{k_r} \tag{10}$$

A plot of $1/r_0$ versus $1/C_0$ as shown in Fig. 13 yields a straight line with an R^2 value of 0.9692, thereby indicating that the initial degradation rates observed obey the Langmuir–Hinshelwood adsorption model for these systems. The values for k_r and K_a were 0.17 mg/L min and 0.04 l/mg, respectively, indicating that photocatalytic degradation is a dominant factor when compared to pollutant adsorption onto the surface of ZnO nanoparticles. This observation suggests that a large specific surface area and reduction in band gap for the catalyst also reduces electron–hole recombination rate and a high degree of crystallinity of these catalysts is responsible for the effectiveness of the photocatalytic degradation capabilities of these materials.

4. Conclusions

ZnO nanoparticle photocatalysis compounds have been synthesized using microwave-assisted combustion and have an average crystalline size of 38 nm with > 93% crystallinity. The extent of photocatalytic degradation of O-NP was monitored using HPLC, and the results indicate that the extent of degradation was affected by the amount of photocatalyst nanoparticles present, the concentration of O-NP, and the pH of solution. It should be noted that in the presence of NaCl, the extent of photocatalytic degradation decreased. Furthermore, the kinetics of photocatalytic degradation of O-NP were shown to fit adequately to a pseudo-first-order kinetic and Langmuir–Hinshelwood model. The results of these studies illustrate that the rate of photocatalytic degradation is constrained by the extent to which the pollutant adsorb to the surface of ZnO nanoparticles.

Acknowledgements

References

[1] J.L. Wang, Microbial Immobilization Techniques and Water Pollution Control, Science Press, Beijing, 2002.

[2] S. Yi, W.Q. Zhuang, B. Wu, S.T.L. Tay, J.H. Tay, Biodegradation of p-nitrophenol by aerobic granules in a sequencing batch reactor, Environ. Sci. Technol. 40 (2006) 2396–2401.

[3] L. Gu, X.W. Zhang, L.C. Lei, Degradation of Aqueous p-nitrophenol by ozonation integrated with activated carbon, Ind. Eng. Chem. Res. 47 (2008) 6809–6815.

[4] S. Yu, J. Hu, J. Wang, Gamma radiation-induced degradation of p-nitrophenol (PNP) in the presence of hydrogen peroxide (H_2O_2) in aqueous solution, J. Hazard. Mater. 177 (2010) 1061–1067.

[5] Y. Liu, D. Wang, B. Sun, Xi. Zhu, Aqueous 4-nitrophenol decomposition and hydrogen peroxide formation induced by contact glow discharge electrolysis, J. Hazard. Mater. 181 (2010) 1010–1015.

[6] US. Environmental Protection Agency, Ambient Water Quality Criteria for Nitrophenols, National Technical Information Service (NTIS), Washington, DC, 1980.

[7] N. Takahashi, T. Nakai, Y. Satoh, Y. Katoh, Variation of biodegradability of nitrogenous organic compounds by ozonation, Water. Res. 28 (1994) 1563–1570.

[8] B. Zhao, G. Mele, I. Pio, J. Li, L. Palmisano, G. Vasapollo, Degradation of 4-nitrophenol (4-NP) using Fe–TiO2 as a heterogeneous photo-Fenton catalyst, J. Hazard. Mater. 176 (2010) 569–574.

[9] E. Marais, T. Nyokong, Adsorption of 4-nitrophenol onto Amberlite® IRA-900 modified with metallophthalocyanines, J. Hazard. Mater. 152 (2008) 293–301.

[10] O.A. O'Connor, L.Y. Young, Toxicity and anaerobic biodegradability of substituted phenols under methanogenic conditions, Environ. Toxicol. Chem. 8 (1989) 853–862.

[11] M.S. Dieckmann, K.A. Gray, A comparison of the degradation of 4-nitrophenol via direct and sensitized photocatalysis in TiO_2 slurries, Water Res. 30 (1996) 1169–1183.

[12] M.A. Oturan, J. Peiroten, P. Chartrin, A.J. Acher, Complete Destruction of p-nitrophenol in aqueous medium by electro-Fenton method, J. Environ. Sci. Technol. 34 (2000) 3474–3479.

[13] L.L. Bo, Y.B. Zhang, X. Quan, B. Zhao, Microwave assisted catalytic oxidation of p-nitrophenol in aqueous solution using carbon-supported copper catalyst, J. Hazard. Mater. 153 (2008) 1201–1206.

[14] M.A. Oturan, J. Peiroten, P. Chartrin, A.J. Acher, Complete Destruction of p-nitrophenol in aqueous medium by electro-Fenton method, Environ. Sci. Technol. 34 (2000) 3474–3479.

[15] N. Modirshahla, M.A. Behnajady, S. Mohammadi-Aghdam, Investigation of the effect of different electrodes and their connections on the removal efficiency of 4-nitrophenol from aqueous solution by electrocoagulation, J. Hazard. Mater. 154 (2008) 778–786.

[16] P. Cañizares, C. Sáez, J. Lobato, M.A. Rodrigo, Electrochemical treatment of 4-nitrophenol-containing aqueous wastes using boron-doped diamond anodes, Ind. Eng. Chem. Res. 43 (2004) 1944–1951.

[17] Y.C. Chang, D.H. Chen, Catalytic reduction of 4-nitrophenol by magnetically recoverable Au nanocatalyst, J. Hazard. Mater. 165 (2009) 664–669.

[18] C.C. Chen, H.J. Fan, Degradation pathways and efficiencies of acid blue 1 by photocatalytic reaction with ZnO nanopowder, J. Phys. Chem. C 112 (31) (2008) 11962–11972.

[19] D.S. Bhatkhande, V.G. Pangarkar, A.A.C.M. Beenackers, Photocatalytic degradation for environmental applications- a review, J. Chem. Technol. Biot. 77 (2002) 102–116.

[20] B. Neppolian, H.C. Choi, S. Sakthivel, B. Arabindoo, V. Murugesan, Solar light induced and TiO_2 assisted degradation of textile dye reactive blue 4, Chemosphere 46 (2002) 1173–1181.

[21] J. Marto, P. São Marcos, T. Trindade, J.A. Labrincha, Photocatalytic decolouration of Orange II by ZnO active layers screen-printed on ceramic tiles, J. Hazard. Mater. 163 (2009) 36–42.

[22] N. Sobana, M. Swaminathan, The effect of operational parameters on the photocatalytic degradation of acid red 18 by ZnO, Sep. Purif. Technol. 56 (2007) 101–107.

[23] Z.L. Wang, J. Song, Piezoelectric Nanogenerators Based on Zinc Oxide Nanowire Arrays, Science 312 (2006) 242–246.

[24] D. Jung, Syntheses and characterizations of transition metal-doped ZnO, Solid State Sci. 12 (2010) 466–470.

[25] S.Y. Chu, T.M. Yan, S.L. Chen, Characteristics of sol–gel synthesis of ZnO-based powders, J. Mater. Sci. Lett. 19 (2000) 349–352.

[26] M.S. Tokumoto, V. Briois, C.V. Santilli, S.H. Pulcinelli, Preparation of ZnO nano particles and colon: Structural study of the molecular precursor, J. Sol–Gel Sci. Techn. 26 (2003) 547–551.

[27] J.H. Kim, W.C. Choi, H.Y. Kim, Y. Kang, Y.K. Park, Preparation of mono-dispersed mixed metal oxide micro hollow spheres by homogeneous precipitation in a micro precipitator, Powder Technol. 153 (2005) 166–175.

[28] L.C. Damonte, L.A. Mendoza Zélis, B. Marí Soucase, M.A. Hernández Fenollosa, Nanoparticles of ZnO obtained by mechanical milling, Powder Technol. 148 (2004) 15–19.

[29] M.L. Kahn, M. Monge, V. Collière, F. Senocq, A. Maisonnat, B. Chaudret, Size- and shape-control of crystalline zinc oxide nanoparticles: A new organometallic synthetic method, Adv. Funct. Mater. 15 (2005) 458–468.

[30] S. Komarneni, M. Bruno, E. Mariani, Synthesis of ZnO with and without microwaves, Mater. Res. Bull. 35 (2000) 1843–1847.

[31] X.Y. Zhao, B.C. Zheng, C.Z. Li, H.C. Gu, Acetate-derived ZnO ultrafine particles synthesized by spray pyrolysis, Powder Technol. 100 (1998) 20–23.

[32] T. Tani, L. Mädler, S.E. Pratsinis, Homogeneous ZnO nano particles by flame spray pyrolysis, J. Nanopart. Res. 4 (2002) 337–343.

[33] Z.R. Dai, Z.W. Pan, Z.L. Wang, Novel nanostructures of functional oxides synthesized by thermal evaporation, Adv. Funct. Mater. 13 (2003) 9–24.

[34] W.Q. Ao, J.Q. Li, H.M. Yang, X.R. Zeng, X.C. Ma, Mechanochemical synthesis of zinc oxide nanocrystalline, Powder Technol. 168 (2006) 148–151.

[35] Y.C. Lee, C.S. Yang, H.J. Huang, S.Y. Hu, J.W. Lee, C.F. Cheng, , C.C. Huang, M.K. Tsai, H.C. Kuang, Structural and optical properties of ZnO nanopowder prepared by microwave-assisted synthesis, J. Lumin. 130 (2010) 1756–1759.

[36] H. Kleinwechter, C. Janzen, J. Knipping, H. Wiggers, P. Roth, Formation and properties of ZnO nano particles from gas phase synthesis processes, J. Mater Sci. 37 (2002) 4349–4360.

[37] N. Daneshvar, S. Aber, M.S. Seyed Dorraji, Photocatalytic degradation of the insecticide diazinon in the presence of prepared nanocrystalline ZnO powders under irradiation of UV–C light, Sep. Purify. Technol. 58 (2007) 91–98.

[38] M.A. Behnajady, N. Modirshahla, R. Hamzavi, Kinetic study on photocatalytic degradation of C.I. Acid Yellow 23 by ZnO photocatalyst, J. Hazard. Mater. 133 (2006) 226–232.

[39] N. Daneshvar, D. Salari, A.R. Khataee, Photocatalytic degradation of azo dye acid red 14 in water on ZnO as an alternative catalyst to TiO_2, J. Photochem. Photobiol. A: Chem. 162 (2004) 317–322.

[40] S. Rabindranathan, S. Devipriya, S. Yesodharan, Photocatalytic degradation of phosphamidon on semiconductor oxides, J. Hazard. Mater. 102 (2003) 217–229.

[41] S. Chakrabarti, B.K. Dutta, Photocatalytic degradation of model textile dyes in wastewater using ZnO as semiconductor catalyst, J. Hazard. Mater. 112 (2004) 269–278.

[42] S. Sakthivel, B. Neppolian, M.V. Shankar, Solar photocatalytic degradation of azo dye: Comparison of photocatalytic efficiency of ZnO and TiO_2, Sol. Energy Mater. Sol. Cells 77 (2003) 65–82.

[43] C. Lizama, J. Freer, J. Baeza, H.D. Mansilla, Optimized photodegradation of Reactive Blue 19 on TiO_2 and ZnO suspensions, Catal. Today 76 (2002) 235–246.

[44] N. Daneshvar, M.A. Behnajady, Y.Z. Asghar, Photooxidative degradation of 4-nitrophenol (4-NP) in UV/H_2O_2 process: Influence of operational parameters and reaction mechanism, J. Hazard. Mater. 139 (2007) 275–279.

[45] D. Hou, L. Feng, J. Zhang, S. Dong, D. Zhou, T.T. Lim, Preparation, characterization and performance of a novel visible light responsive spherical activated carbon-supported and Er^{3+}:$YFeO_3$-doped TiO_2 photocatalyst, J. Hazard. Mater. 199–200 (2012) 301–308.

[46] U.G. Akpan, B.H. Hameed, Photocatalytic degradation of 2,4-dichlorophenoxyacetic acid by Ca–Ce–W–TiO_2 composite photocatalyst, Chem. Engin. J. 173 (2011) 369–375.